On the Momentum, Vorticity and Mass Balance on the Oregon Shelf

J. S. ALLEN AND PIJUSH K. KUNDU[1]

School of Oceanography, Oregon State University, Corvallis 97331

(Manuscript received 23 May 1977, in final form 25 July 1977)

ABSTRACT

Velocity measurements from the continental shelf off Oregon taken during the Coastal Upwelling Experiment CUE-2 in the summer of 1973 are utilized to investigate momentum, vorticity and mass balance relationships for subinertial frequency ($\omega < 0.6$ cpd) current fluctuations. Measurements from stations in water of depths of 54, 100 and 200 m are utilized. By a comparison of the magnitude of terms involving horizontal velocities in the linear momentum and in the nonlinear, depth-integrated momentum equations, support is found for the linear geostrophic balance of the alongshore velocity in the onshore-offshore momentum equation and, in the depth range 100 m $\leq H \leq$ 200 m, for a linear ageostrophic balance in the alongshore momentum equation. Evidence is also found to support the validity of a linear depth-integrated vorticity balance, again for depths 100 m $\leq H \leq$ 200 m. In this balance, which is similar to that in the theory for continental shelf waves, the interaction of the onshore velocity with the onshore-offshore bottom slope of the continental shelf forms the primary vortex stretching mechanism. The mass balance equation from idealized two-dimensional coastal upwelling models, wherein the depth integral of the interior, inviscid onshore velocity U equals the offshore Ekman layer transport $-\tau/\rho_0 f$, where τ is the alongshore component of the wind stress, is investigated by comparing the time-dependent behavior of U and $\tau/\rho_0 f$. It is found that the correlation of U and $\tau/\rho_0 f$ is of the proper sign to support this relation and that, in general, the magnitudes of these two terms are similar, but that the correlation is not especially high, presumably due to three-dimensional effects.

1. Introduction

In this investigation we analyze velocity measurements from the continental shelf off Oregon taken during the Coastal Upwelling Experiment CUE-2 in 1973 to examine some characteristics of the momentum, vorticity and mass balances which are frequently utilized in theoretical or conceptual models of the coastal flow regime.

The set of theoretical models with which we will be concerned are those for subinertial frequency, time-dependent motion on the continental shelf and slope which describe the flow, away from surface friction layers, as linear and inviscid and which include, as a forcing mechanism, the alongshore component of the wind stress at the coast (e.g., Walin, 1972; Gill and Schumann, 1974; Gill and Clarke, 1974; Allen, 1976). These models involve forced coastal trapped waves. Depending on the exact assumptions about the stratification and shelf topography, the forced waves may be barotropic continental shelf waves, internal Kelvin waves or more general, coupled forms of these two types of wave modes (Allen, 1975; Wang and Mooers, 1976). A growing number of recent observational studies seem to indicate that the time-dependent response to atmospheric forcing of water in some coastal regions, such as that off Oregon, may be approximately described by these theoretical models. This appears to be especially true with regard to the prediction of the behavior of the barotropic component of the alongshore velocity field by the theory for forced and free continental shelf waves (Smith, 1974; Kundu *et al.*, 1975; Huyer *et al.*, 1975; Kundu and Allen, 1976).

A feature which is common to several of the theoretical models of this type is the assumption that the relevant alongshore spatial scales are larger than the onshore-offshore scales. It follows, through scaling arguments, that the lowest order onshore-offshore momentum balance is geostrophic, i.e., that the alongshore velocity component is in geostrophic balance. An additional common feature is the assumption that the time variations are such that the alongshore momentum balance is ageostrophic. In particular, if we consider a Cartesian coordinate system (x,y,z), with corresponding velocity components (u,v,w), aligned so that the x axis is in the onshore-offshore direction, the y axis is alongshore and the z axis vertical, the above assumptions imply that the lowest order x and y momentum balances are

[1] Present affiliation: Ocean Sciences Center, Nova University, Dania, Fla. 33004.

0022-3670/78/0013-0027$07.50

$$fv = p_x, \tag{1.1a}$$

$$v_t + fu = -p_y, \tag{1.1b}$$

where p is the pressure divided by a reference density ρ_0, t is time, f is the constant Coriolis parameter, and the subscripts (x,y,t) denote partial differentiation.

The importance of the ageostrophic term v_t in (1.1b) in the theory for barotropic continental shelf waves has been emphasized by Gill and Schumann (1974). The ageostrophic term is important also in stratified coastal models (e.g., Walin, 1972; Gill and Clarke, 1974; Allen, 1976), since v_t is an essential part of the lowest order balance for free and forced internal Kelvin waves. For example, in a free internal Kelvin wave, $u = 0$ and the balance in (1.1b) is $v_t = -p_y$.

Note that the substitution of (1.1a,b) in the continuity equation

$$u_x + v_y + w_z = 0 \tag{1.2}$$

gives

$$w_z = f^{-1}v_{xt}, \tag{1.3}$$

and that the lowest order flow is horizontally divergent. Eqs. (1.1a,b) and (1.3) differ, of course, from the usual assumption for low-frequency mid-ocean motions of geostrophic balance and, consequently, of horizontal nondivergence at lowest order.

An additional fundamental balance, from which a governing equation is usually obtained, is that for vorticity. One useful form of vorticity equation may be derived by depth-integrating (1.3). For example, if we consider the barotropic motion over a continental shelf where the depth $H = H(x)$ is independent of the alongshore coordinate y, the top surface is bounded by a rigid lid (Gill and Schumann, 1974), and there is negligible suction into the surface Ekman layer, the depth integrated form of (1.3) is

$$v_{xt} = (H_x/H)fu. \tag{1.4}$$

Eq. (1.4) expresses the time rate of change of vorticity v_x due to the stretching of fluid columns by the motion of the fluid up or down the bottom slope of the continental margin. This vortex stretching provides the mechanism for continental shelf waves.

The conservation of mass provides another basic balance in coastal regions. This balance is extremely important for the study of coastal upwelling. The simplest conceptual form of mass balance on the continental shelf results from an assumption of two-dimensional flow, i.e., an assumption of zero velocity gradients in the alongshore direction. In that case, with the rigid lid approximation, the net onshore-offshore mass flux at a position x on the shelf is equal to zero, i.e.,

$$\int_{-H}^{0} u_T dz = 0, \tag{1.5}$$

where u_T is the total onshore-offshore velocity component. If we assume that x is located offshore of the region where there is appreciable vertical motion into the surface Ekman layer and that the onshore velocity u_T may be divided into an inviscid component u and a frictional component which is confined to a thin surface layer, then (1.5) reduces to

$$\int_{-H}^{0} u dz = -\tau/f\rho_0, \tag{1.6}$$

where τ is the alongshore component of the wind stress at the coast (assumed not to vary appreciably on the onshore-offshore spatial scales considered here) and $-\tau/f\rho_0$ is the offshore transport in the surface Ekman layer.

Eqs. (1.5) and (1.6) are strong constraints which are accompanied by a simple conceptual picture of the onshore-offshore mass balance. If alongshore velocity gradients are appreciable, however, then the two-dimensional approximation will, of course, be violated and (1.5) and (1.6) will not hold.

In this study, we analyze velocity measurements from the coastal upwelling experiment CUE-2 off Oregon in the summer of 1973 in an attempt to investigate the validity of the time-dependent momentum (1.1a,b) and vorticity balances (1.4), utilized in theoretical models, and the two-dimensional mass balance (1.6), frequently utilized in conceptual models of coastal upwelling.

2. Observations

The locations of the current meter moorings in CUE-2 are described in Kundu and Allen (1976). Here we utilize velocity measurements from stations Aster, Carnation and Edelweiss, located on an east-west (onshore-offshore) line at 45°16′N in water of depth 54, 100 and 200 m, respectively (see Fig. 1). The east-west line is approximately perpendicular to the coastline and local isobaths. Currents and temperatures were measured with Aanderaa current meters tethered to subsurface moorings. Winds were measured at Newport, Ore. (44°37′N).

The measurement depths are given in Table 1[2]. The record lengths are Aster, 29 June–26 August (58 days); Carnation, 30 June–28 August (59 days); Edelweiss, 22 July–28 August (37 days). Note that the records at Edelweiss are approximately

[2] Measurements at Aster were previously reported in Kundu and Allen (1976) to be at 20 and 40 m in water of depth 50 m. The Aster measurements were, more accurately, at 24 and 44 m in water of depth 54 m.

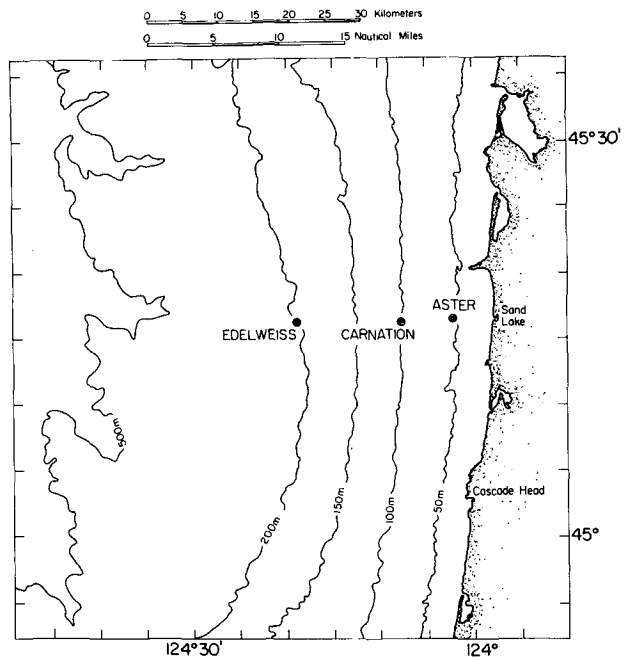

FIG. 1. Location of current meter stations.

22 days shorter than those at Aster and Carnation. The data processing is described in detail in Pillsbury *et al.* (1974) and Smith (1974). It includes filtering of the 5–10 min observations to obtain hourly time series and refiltering these to eliminate the tidal and inertial frequencies by means of a filter having 121 weights with a half-power point of 40 h [0.6 cycle per day (cpd)]. The resulting series was then decimated to 6 h values. We will be concerned here, therefore, with frequencies $\omega < 0.6$ cpd.

For reference, the means, standard deviations and principal axes for the eastward (u) and northward (v) velocities, computed for the respective record lengths (from Kundu and Allen, 1976), are given in Table 1. The time mean of a variable is denoted by an overbar and the standard deviation by a prime, e.g.,

$$u(\mathbf{x},t) = \overline{u(\mathbf{x})} + \hat{u}(\mathbf{x},t), \quad \hat{u}' = (\overline{\hat{u}^2})^{1/2}, \quad (2.1a,b)$$

where $\hat{u}$ is the time fluctuation. For simplicity in notation, the caret on $\hat{u}$ is dropped when referring to the measurements in Sections 4–7 where all variables without an overbar are considered to have the time mean removed.

It may be seen in Table 1 that the major principal axes at Aster and Carnation deviate from north by only a few degrees. For the analysis here, therefore, we will use a Cartesian coordinate system (x,y,z) with the alongshore coordinate y aligned north-south, positive northward, with the onshore-offshore coordinate x aligned east-west, positive eastward, and with z aligned vertically, positive upward. The corresponding velocity components are (u,v,w), respectively.

The density in this region is strongly controlled by the salinity. Although time series measurements of the temperature were made at the current meters, corresponding measurements of the salinity were not made; therefore, time series of density are not available.

For use in connection with (1.6) and the mass balance investigation, the north-south component of the wind stress at Newport was computed from the hourly values of the wind stress vector and then low-pass filtered in the same manner as the currents. The formula used is $\tau = \rho_A C_D(u_W^2 + v_W^2)^{1/2} \times v_W$ [dyn cm^{-2}], where (u_W,v_W) are the wind velocity components, $\rho_A = 1.2 \times 10^3$ g cm^{-3} is the air density and $C_D = 1.4 \times 10^{-3}$.

3. Analysis

We assume that the motion away from surface frictional layers is inviscid and is governed by the equations

$$u_x + v_y + w_z = 0, \quad (3.1a)$$

$$u_t + \mathbf{u}\cdot\nabla u - fv = -p_x, \quad (3.1b)$$

$$v_t + \mathbf{u}\cdot\nabla v + fu = -p_y, \quad (3.1c)$$

$$0 = -p_z - g\rho/\rho_0, \quad (3.1d)$$

where the Boussinesq approximation has been made, ρ is the perturbation density such that the total density $\rho_T = \rho_0 + \rho$ where ρ_0 is a constant reference density ($\rho_0 = 1$ g cm^{-3}), $\rho_0 p$ is the difference in pressure from a hydrostatic state with uniform density ρ_0, i.e., $p = \rho_0^{-1} p_T + gz$ where p_T is the total pressure, g is the acceleration of

TABLE 1. Means, standard deviations and principal axes.

Station	Depth (m)	$\bar{u}$ (cm s^{-1})	$\bar{v}$ (cm s^{-1})	u' (cm s^{-1})	v' (cm s^{-1})	Major principal axis* (deg)
Aster	24	6.0	−11.3	4.0	12.5	1
	44	−0.6	−0.9	1.6	9.4	3
Carnation	20	3.2	−23.9	4.7	10.0	1
	40	4.3	−10.9	3.0	10.5	2
	60	2.7	−2.0	2.9	11.7	1
	80	1.1	2.9	2.0	10.7	4
	95	0.6	2.5	1.7	8.4	6
Edelweiss	20	2.4	−21.7	4.3	6.1	32
	80	2.6	−4.6	2.3	5.5	11
	120	2.0	2.5	1.9	5.4	2
	180	−1.8	7.3	1.7	5.4	12
	195	−1.7	5.5	2.4	4.9	22

* Measured counterclockwise from north.

gravity and $\mathbf{u}$ the velocity vector with components (u,v,w). The fluid may be stratified and in general the perturbation density is a function of the spatial coordinates and time, i.e., $\rho = \rho(x,y,z,t)$. An additional equation for ρ is required, of course, to form a complete set of governing equations. Because of a lack of time series measurements of density, the time-dependent behavior of ρ will not be considered and an equation for ρ will not be utilized here. Velocity measurements will be used to investigate balances implied by the continuity and momentum equations (3.1).

Below we derive various approximate forms of (3.1) which are used in coastal problems. We also derive approximate depth-integrated equations from (3.1) and form a depth-integrated vorticity equation. The time scale of interest δ_t is considered to be larger than an inertial period[3], i.e.,

$$\delta_t \gg f^{-1}. \tag{3.2}$$

The fluid is assumed to be bounded by a rigid upper surface at $z = 0$ and a variable depth bottom surface at $z = -H(x,y)$. The inviscid interior flow is assumed to extend in depth from $z = -H$ to $z = -H_S$ where H_S is a constant depth of the surface frictional layer.

One frequently used scaling argument for coastal problems is that the characteristic alongshore spatial scale δ_y is larger than the characteristic onshore-offshore scale δ_x, i.e.,

$$\delta_y \gg \delta_x. \tag{3.3}$$

With (3.3), the order-of-magnitude estimate $u \approx (\delta_x/\delta_y)v$, obtained from the continuity equation (3.1a), implies that $u \ll v$. Assumptions (3.2) and (3.3) then lead to the following approximate forms of (3.1b) and (3.1c):

$$fv = p_x, \tag{3.4a}$$

$$v_t + \mathbf{u}\cdot\nabla v + fu = -p_y, \tag{3.4b}$$

where the v_t term has been retained by the assumption that $f\delta_t \approx v/u$.

The standard linear form of (3.4b),

$$v_t + fu = -p_y, \tag{3.5a}$$

results from the additional assumption of small Rossby number, i.e., of $V_0/f\delta_x \ll 1$ where V_0 is a characteristic alongshore velocity. Alternatively, without the use of (3.3) first, the small Rossby number approximation may be applied directly to (3.1) to give, as the two momentum equations, (3.5a) and the linear form of (3.1b),

$$u_t - fv = -p_x. \tag{3.5b}$$

[3] Possible Reynolds stress effects from higher frequency components of the motion are not considered here.

We now consider the vorticity balance. Because we are not working with an additional equation for the density we are not able to form an equation for the potential vorticity. It is possible, however, to form a depth-integrated vorticity equation from the continuity and momentum equations alone. The depth integration in this case is over the supposed region of inviscid flow, i.e., $-H \leq z \leq -H_S$. In cases where the flow is barotropic this equation reduces to the appropriate governing vorticity equation. It also directly expresses the effect of vortex stretching by the interaction of the bottom velocities and the bottom slope, which is the essential mechanism in continental shelf waves. To form a depth-integrated vorticity equation it is convenient to first integrate the continuity and momentum equations (3.1) over z from $z = -H(x,y)$ to $z = -H_S$. It is assumed that there is negligible suction into the surface layer, i.e., that $w(z = -H_S) \approx 0$, and that at $z = -H$ the flow satisfies the inviscid boundary condition $w = -\mathbf{u}\cdot\nabla H$. Utilizing the continuity equation (3.1a) to first express the nonlinear terms in (3.1b) and (3.1c) in divergence form, we obtain

$$U_x + V_y = 0, \tag{3.6a}$$

$$U_t + NL^x - fV = -P_x + H_x p_B, \tag{3.6b}$$

$$V_t + NL^y + fU = -P_y + H_y p_B, \tag{3.6c}$$

where

$$(U,V,P) = \int_{-H}^{-H_S} (u,v,p)\,dz, \tag{3.7a}$$

$$NL^x = \left(\int u^2 dz\right)_x + \left(\int uv dz\right)_y, \tag{3.7b}$$

$$NL^y = \left(\int uv dz\right)_x + \left(\int v^2 dz\right)_y, \tag{3.7c}$$

$$p_B = p(z = -H). \tag{3.7d}$$

The integrals over z in (3.7b) and (3.7c) and in subsequent equations are understood to be from $-H$ to $-H_S$, as in (3.7a). Depth averages, defined by

$$\langle v\rangle = V/H_E, \quad \langle u\rangle = U/H_E, \tag{3.8a,b}$$

where $H_E = H - H_S$, are also utilized later.

The depth-integrated momentum equations are also useful to work with in an attempt to evaluate the relative size of the nonlinear terms. A direct calculation of the nonlinear terms in (3.1b) and (3.1c) is hard to accomplish. In addition to the difficulty in a coastal region of evaluating horizontal velocity derivatives at fixed values of z, the ageostrophic balance (3.4b) or (3.5a) implies that the motion is horizontally divergent to lowest order. This means, for example, in (3.1c)

that the wv_z term in $\mathbf{u}\cdot\nabla v$ will formally be of the same order of magnitude as the other two terms uv_x and vv_y which involve horizontal velocities. Since w is not measured, that term cannot be directly calculated. The depth integration, of course, eliminates w and results in expressions in terms of horizontal velocities only.

The evaluation of the nonlinear terms (3.7b,c) in (3.6b,c) requires the calculation of alongshore derivatives. Although there were velocity measurements in CUE-2 from moorings displaced alongshore, it is felt that the spacing of these moorings and, more importantly, the large gradients in the flow in the onshore-offshore direction relative to those in the alongshore direction (Kundu and Allen, 1976), make a direct evaluation of y derivatives impractical.

It is possible, however, to make some progress in the estimation of the term $(\int v^2 dz)_y$ in NL^y with the use of two ad hoc assumptions. Since it is expected, based on the results (3.4a,b) of the scale analysis utilizing (3.3), that the nonlinear terms in the y momentum equation will be relatively more important than those in the x momentum equation, an approximate evaluation of NL^y should be helpful. If it is assumed that

$$H_y \approx 0, \quad v_z \approx 0, \tag{3.9a,b}$$

it is possible to relate the y derivative in (3.7c) to an x derivative through the continuity equation (3.6a). Eq. (3.9a) can be justified, to some extent, by the form of the topography in this region (Fig. 1), by the fact that the orientation of the principal axes of the fluctuation is nearly along the y axis, and by some of the results in Section 5. Assumption (3.9b) is partially rationalized by the fact that the fluctuating alongshore velocity components at Carnation and Edelweiss have been found to be very nearly depth-independent (Kundu *et al.*, 1975; Kundu and Allen, 1976). That behavior is illustrated by the nearly depth-independent values of v' in Table 1.

With assumptions (3.9a,b) and with (3.6a), we obtain

$$\left(\int v^2 dz\right)_y \approx -2\langle v\rangle\left(\int u dz\right)_x, \tag{3.10}$$

so that

$$NL^y \approx NL^y_A = \left(\int uv dz\right)_x - 2\langle v\rangle U_x, \tag{3.11}$$

and NL^y_A may be evaluated using x derivatives only.

A mass transport vorticity equation may be obtained by cross differentiating (3.6b) and (3.6c):

$$(V_x - U_y)_t + NL^y_x - NL^x_y = -H_x p_{By} + H_y p_{Bx}, \tag{3.12}$$

where approximations (3.9) have not been used. If we appeal to the order-of-magnitude arguments based on (3.3), which result in an assumption of geostrophic balance for v in (3.4a), Eq. (3.12) may be simplified to

$$V_{xt} + NL^y_x = -H_x p_{By} + H_y f v_B. \tag{3.13}$$

Since the results in Section 4 support the geostrophic balance (3.4a), it is expected that (3.13) will be a relevant approximation to (3.12).

The term on the right-hand side of (3.13) involving p_{By} may be expressed in terms of velocities with the use of the momentum equation (3.4b). An evaluation of the nonlinear terms in (3.4b) is again impractical using present velocity measurements and, to proceed, an additional approximation is required. It is found in Section 4 that, in the momentum equation (3.6c), the nonlinear term NL^y is generally smaller than the linear terms. We appeal to that result to justify the use of the linear momentum equation (3.5a) in the substitution for p_{By} and to justify the neglect in (3.13) of NL^y_x relative to V_{xt}. In the neglect of NL^y_x it is assumed that V_t and NL^y do not change their relative magnitude when x derivatives are taken. Consequently, with the use of (3.5a) and (3.8a) we may write (3.13) as an approximate linear, depth integrated vorticity equation:

$$\langle v\rangle_{xt} = (H_x/H_E)(fu_B + v_{Bt} - \langle v\rangle_t) + (H_y/H_E) f v_B. \tag{3.14}$$

4. Momentum balance

We first investigate the balances in the linear form of the momentum equations (3.5a) and (3.5b) by comparing the relative size of the velocity terms v_t, fu and u_t, fv.

The time derivatives in (3.5a) and (3.5b) are approximated by applying a central difference approximation, with a time increment of 6 h to the (low pass filtered) data. For example, we use

$$v_t(t) \approx \Delta_t v = [v(t + \Delta t) - v(t - \Delta t)]/2\Delta t, \tag{4.1}$$

where $\Delta t = 6$ h. Errors from the time-difference approximation are discussed in Appendix B.

Time variations of v_t, fu, u_t and fv from the data at Car 80 (the current meter at depth 80 m at station Carnation) are given in Fig. 2. The appropriate combinations of these terms, which appear in (3.5), are denoted by

$$Y_T = v_t + fu, \quad X_T = u_t - fv \tag{4.2a,b}$$

and Y_T is also plotted. In addition, included for comparison is a plot of the alongshore component of the wind stress (with the mean $\bar{\tau} = -0.37$ dyn cm^{-2} removed). It may be seen that at Car 80 v_t and fu are of the same magnitude and that there is

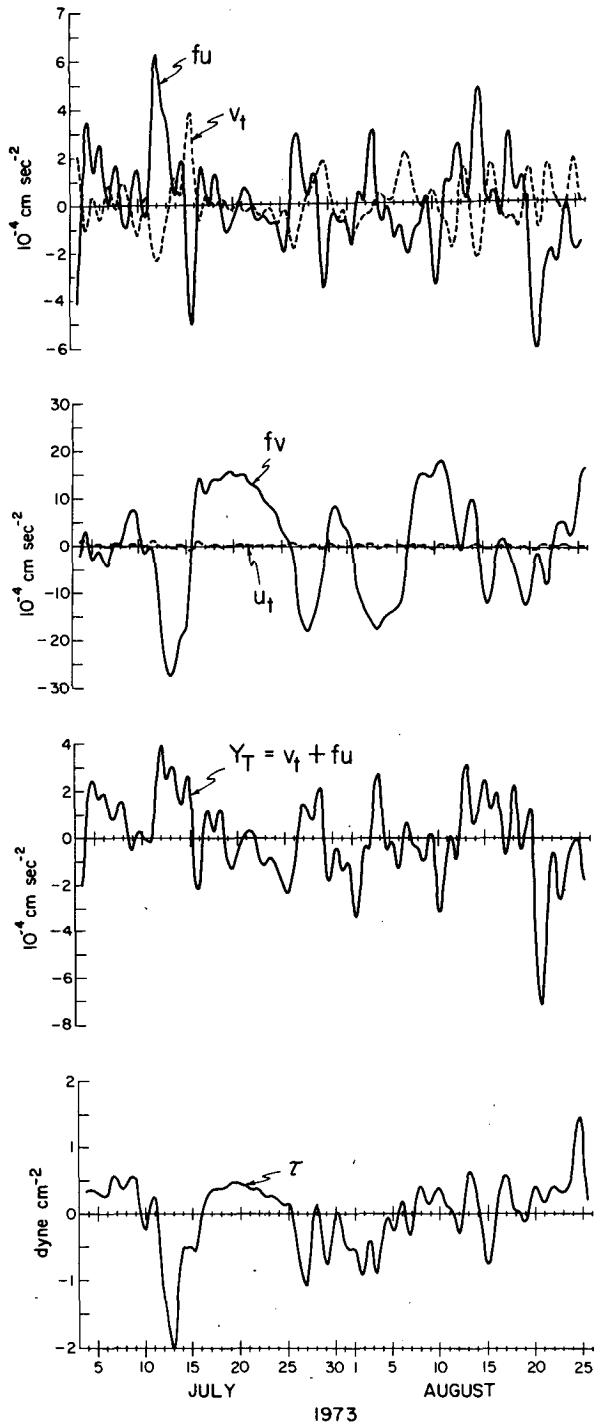

FIG. 2. Time series of v_t, fu, u_t, fv and $Y_T = v_t + fu$ at Carnation (80 m) and of the north-south component of the wind stress τ at Newport.

a clear tendency for these two terms to balance each other. In contrast, it may also be seen that in general fv has a substantially larger magnitude than u_t and that, as a result, the term u_t could not be important in the x momentum equation.

The standard deviations of the terms v_t, fu, u_t, fv, X_T and the ratios v_t'/fu', u_t'/fv' are given in Table 2 for the different stations. The normalized cross-correlation coefficients between v_t and fu and between u_t and fv, denoted by brackets, e.g., $\{v_t,fu\} = \overline{v_t fu}/v_t' fu'$, are also given. The statistical significance of the correlation coefficients is discussed in Appendix A. The time periods covered in the calculations with the low-passed data are Aster, 2 July–24 August (53 days); Carnation, 3 July–25 August (54 days); Edelweiss, 27 July to 25 August (30 days).

The impressions from Fig. 2 are borne out by the standard deviations (SD's) and correlation coefficients. At Car 80, v_t and fu are significantly negatively correlated and have SD's of similar magnitude, with the SD of fu being larger. It may be expected, therefore, that these terms have some tendency to balance and to cancel each other in the sum Y_T. This is the case and the SD of Y_T is smaller than that of fu.

In general, the standard deviation of fu is somewhat larger than that of v_t for all the measurement points. At each station the SD of v_t is closer in magnitude to that of fu at the deeper current meters, with the exception of the very bottom current meters at Carnation and Edelweiss. The SD of v_t is fairly uniform with depth while that of fu increases in magnitude as the depth decreases. This trend is illustrated in Table 2 by the variations in v_t'/fu' with depth and could be anticipated from the relative depth independence of v' and the general increase of u' at shallower depths (Table 1). The absolute value of the cross-correlation coefficient $\{v_t,fu\}$ also tends to be larger at the deeper points. If, as in (3.5a), p_y is the term that balances Y_T,[4] then evidently there are baroclinic contributions to the alongshore pressure gradient which result in an increase in the magnitude of p_y for decreasing depth. This would imply that the fraction of the onshore flow which is geostrophically balanced increases at the shallower depths (below the surface layer).

At all three stations $\{v_t,fu\}$ falls to near zero values at 20 m. This presumably reflects the fact that additional physical effects, not included in (3.5a) and (3.5b), enter the momentum balance at 20 m. These effects are probably the result of turbulent frictional processes associated with the surface layer. At the bottom current meters at Carnation and Edelweiss, there is a decrease of the ratio v_t'/fu' and the correlation $\{v_t,fu\}$, which is probably due to frictional effects from the bottom

[4] The possibility of using coastal sea level measurements from a set of tide gages along the Oregon coast to obtain information about p_y is being investigated by Dr. A. Huyer (private communication).

TABLE 2. Standard deviations and cross-correlation coefficients.

Station	Depth (m)	v_t'	fu' (10^{-4} cm s^{-2})	Y_T'	$\frac{v_t'}{fu'}$	$\{v_t, fu\}$	u_t'	fv' (10^{-4} cm s^{-2})	X_T'	$\frac{u_t'}{fv'}$	$\{u_t, fv\}$
Aster	24	1.15	4.12	4.35	0.28	0.07	0.59	12.79	12.85	0.05	−0.08
	44	0.90	1.65	1.70	0.55	−0.21	0.23	9.71	9.68	0.02	0.14
Carnation	20	0.98	4.81	4.91	0.20	0.00	0.68	10.24	10.26	0.07	0.01
	40	0.96	3.09	2.96	0.31	−0.29	0.47	10.83	10.77	0.04	0.15
	60	1.15	2.95	2.68	0.39	−0.42	0.52	12.01	11.91	0.04	0.21
	80	1.01	2.01	1.70	0.50	−0.53	0.37	10.98	10.90	0.03	0.25
	95	0.75	1.69	1.53	0.44	−0.43	0.25	8.70	8.64	0.03	0.25
Edelweiss	20	0.60	3.81	3.90	0.16	0.05	0.47	5.76	5.73	0.08	0.11
	80	0.62	2.18	2.04	0.28	−0.36	0.37	5.04	4.93	0.07	0.34
	120	0.75	1.99	1.91	0.38	−0.29	0.40	5.48	5.39	0.07	0.24
	180	0.74	1.73	1.58	0.43	−0.40	0.35	5.52	5.42	0.06	0.32
	195	0.66	2.30	2.20	0.29	−0.30	0.38	5.03	4.92	0.08	0.32

boundary layer (Kundu, 1976). At Aster 40, v_t'/fu' obtains the largest value measured, but $\{v_t, fu\}$ is lower than at the mid-depth or bottom points at Carnation or Edelweiss. Again, additional effects, perhaps frictional, may be operative in the shallow water at Aster.

Since the fluctuating v components of velocity are approximately depth-independent and are highly correlated, both in depth and onshore-offshore (Kundu and Allen, 1976), the time variation of v should be similar to that of $\langle v \rangle_x$. It seems, therefore, that the relatively high correlation of v_t and fu at the points near the bottom perhaps indicates the presence of a vorticity balance like (3.14), where a correlation between $\langle v \rangle_{xt}$ and u_B would be expected. The vorticity balance is investigated in Section 5.

The results in Table 2 for the SD's of v_t and fu strongly support the inclusion of the ageostrophic term v_t in the y momentum balance equation (3.5a). On the other hand, the magnitudes of the SD's of u_t in Table 3 are generally much smaller than those of fv which justifies the neglect of the ageostrophic term u_t in (3.4a). This result, together with the previously found high correlation of v and coastal sea level (Smith, 1974; Kundu *et al.*, 1975) supports the assumption of geostrophic balance for fv. It should be noted that the assumptions of geostrophic balance in (3.4a) and ageostrophic balance in (3.5a) lead to the long-wave (nondispersive) approximation for continental shelf waves (Gill and Schumann, 1974). The above results, consequently, tend to support the long-wave approximation.

By comparing in Fig. 2 the variation of the wind stress τ with that of v_t and fu at Car 80 we may make some additional comments. If a linear, two-dimensional balance is present in (3.5a), v_t and fu will balance exactly, with $p_y = 0$. The occurrence of the type of balance during some time periods would be indicated by relatively small values of Y_T. It may be seen from Fig. 2 that there is no obvious relation between the variation of τ and of Y_T. Halpern (1976) has speculated that there may be an increased tendency toward a two-dimensional *mass* balance during strong wind events. In contrast, it appears from Fig. 2 that there is no evidence for a tendency toward a two-dimensional *dynamic* balance during periods when the wind stress is of large magnitude.

We next attempt to estimate the size of the nonlinear terms in the depth-integrated momentum equations (3.6b) and (3.6c). It is convenient to

TABLE 3. Standard deviations (10^{-4} cm s^{-2}) and cross-correlation coefficients from (4.6a) and (4.6b) at points EC and CA.

	$\langle u \rangle_t'$	$f\langle v \rangle'$	$\tilde{X}_L'$	$NL_A^{x\prime}$	$\tilde{X}_T'$		
EC	0.25	6.61	6.48	0.05	6.49		
CA	0.24	9.93	9.86	0.18	9.84		
	$\langle v \rangle_t'$	$f\langle u \rangle'$	$\tilde{Y}_L'$	$NL_A^{y\prime}$	$NL_1^{y\prime}$	$NL_2^{y\prime}$	$\tilde{Y}_T'$
EC	0.73	1.65	1.30	0.12	0.07	0.14	1.30
CA	0.87	1.67	1.45	0.38	0.37	0.67	1.49
	$\{\langle v \rangle_t, f\langle u \rangle\}$	$\{\tilde{Y}_L, NL_A^y\}$	$\{\tilde{Y}_L, NL_1^y\}$	$\{\tilde{Y}_L, NL_2^y\}$	$\{NL_1^y, NL_2^y\}$	$\{\langle u \rangle_t, f\langle v \rangle\}$	$\{f\langle v \rangle, NL_A^x\}$
EC	−0.66	−0.01	−0.18	0.08	−0.54	0.53	−0.10
CA	−0.50	−0.04	0.39	−0.24	−0.89	0.31	0.10

work with the velocities in the linear terms expressed as depth averages (3.8). In terms of these, the left hand sides of (3.6b) and (3.6c) may be written

$$\langle u\rangle_t + H_E^{-1}\left[\left(\int u^2 dz\right)_x + \left(\int uv dz\right)_y\right] - f\langle v\rangle = \tilde{X}_T, \quad (4.3a)$$

$$\langle v\rangle_t + H_E^{-1}\left[\left(\int uv dz\right)_x - 2\langle v\rangle\left(\int u dz\right)_x\right] + f\langle u\rangle = \tilde{Y}_T, \quad (4.3b)$$

where NL_A^y (3.11) has been used in place of NL^y.

For the calculation of the depth averages in (4.3) it is necessary to estimate the depth H_S of the surface frictional layer. The measurements of the u velocities at Carnation (Fig. 5 of Kundu *et al.*, 1975; Fig. 6 of Huyer, 1976) indicate that the onshore-offshore currents at 20 m sometimes flow, as do the near-surface currents, in a direction opposite to the motion at the deeper current meters. At other times, the 20 m and the deeper u velocities have the same sign and similar time variability. It appears that the effects from the surface frictional layer occasionally influence the currents at 20 m. This feature is also indicated by the variation of the cross-correlation coefficients of u at Carnation as a function of vertical separation. The cross-correlation coefficients between u_{40} (u at 40 m) and u_{60}, u_{80}, u_{95} are higher (~0.65) than that between u_{20} and u_{40} (~0.5). Additional indications of surface layer effects on the 20 m currents were just mentioned in connection with the results in Table 2 and more will be discussed in Section 6. As for the extent of penetration of frictional effects, a rough estimate, sufficient for our purposes, of 20 m for the mean depth of the surface layer at Carnation may be obtained from the plot of u velocities in Fig. 6 of Huyer (1976) or from the hodograph of current vectors in Kundu (1977). Based on the above considerations, we assume that $H_S = 20$ m and we omit the 20 m current meter records in forming the depth integrals.

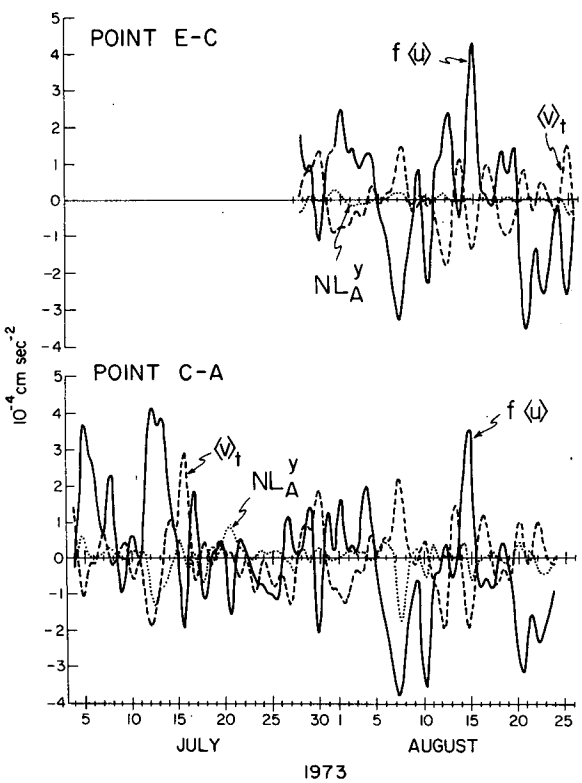

FIG. 3. Time series of $\langle v\rangle_t$, $f\langle u\rangle$ and NL_A^y in Eq. (4.6b) at points EC and CA.

A simple trapezoidal approximation is used for calculating the depth averages. The resulting formulas, e.g., for u, are

$$\left.\begin{aligned} &\text{Aster:} && \langle u\rangle = u_{44} \\ &\text{Carnation:} && \langle u\rangle = (30u_{40} + 20u_{60} + 17.5u_{80} + 12.5u_{95})/80 \\ &\text{Edelweiss:} && \langle u\rangle = (80u_{80} + 50u_{120} + 37.5u_{180} + 12.5u_{195})/180 \end{aligned}\right\}. \quad (4.4)$$

The depth integrals needed in the nonlinear terms, such as $U = H_E\langle u\rangle$, are calculated from (4.4) by multiplying by the appropriate H_E.

It is not possible to evaluate directly the y derivative term in NL^x in (4.3a). Based on the results in Table 2 and on the scaling arguments that led to (3.4a), however, it might be anticipated that the term NL^x will be small relative to fV. We will, therefore, be satisfied in the evaluation of terms in (4.3a) to calculate only that part of the nonlinear term which involves the x derivative and which may be readily approximated.

The terms in (4.3a) and (4.3b) are calculated from difference approximations centered at a point x_0 half way between two stations which are separated by a distance $2\Delta x$. With the notation

$$\bar{\phi}^x = \tfrac{1}{2}[\phi(x_0 + \Delta x) + \phi(x_0 - \Delta x)], \quad (4.5a)$$

$$\Delta_x\phi = [\phi(x_0 + \Delta x) - \phi(x_0 - \Delta x)]/2\Delta x, \quad (4.5b)$$

the difference approximations for (4.3a) and (4.3b) at the point x_0 are

$$\langle \bar{u} \rangle_t^x + NL_A^x - f\langle \bar{v} \rangle^x = \tilde{X}_T, \quad (4.6a)$$

$$\langle \bar{v} \rangle_t^x + NL_A^y + f\langle \bar{u} \rangle^x = \tilde{Y}_T, \quad (4.6b)$$

where

$$NL_A^x = \left[\Delta_x\left(\int u^2 dz\right)\right]/\bar{H}_E^x, \quad (4.7a)$$

$$NL_A^y = NL_1^y + NL_2^y, \quad (4.7b)$$

$$NL_1^y = \left[\Delta_x\left(\int uv dz\right)\right]/\bar{H}_E^x,$$

$$NL_2^y = -2\langle \bar{v} \rangle^x \left[\Delta_x\left(\int u dz\right)\right]/\bar{H}_E^x, \quad (4.7c,d)$$

and where the y derivative term in NL^x has been omitted. The time derivatives are calculated as before by (4.1). The notation

$$\tilde{X}_L = \langle \bar{u} \rangle_t^x - f\langle \bar{v} \rangle^x,$$

$$\tilde{Y}_L = \langle \bar{v} \rangle_t^x + f\langle \bar{u} \rangle^x, \quad (4.8a,b)$$

is used for the linear terms in (4.6a,b).

The results from the point x_0 between Edelweiss and Carnation are denoted by EC and those for the point between Carnation and Aster by CA. For EC, $2\Delta x = 15.5$ km and for CA, $2\Delta x = 7.1$ km. The time period covered in the calculations at EC is 27 July–25 August (30 days) and the period at CA is 3 July–23 August (51 days).

The standard deviations and the cross correlation coefficients for the various terms are given in Table 3. In the x momentum equation (4.6a), similar to the previous results for u_t and fv, we find that $\langle u \rangle_t'$ is small compared with $f\langle v \rangle'$. These results further support the approximation of geostrophic balance for v in (3.4a).

For the y momentum equation (4.6b), the results for $\langle v \rangle_t$ and $f\langle u \rangle$ are also similar to those obtained before for v_t and fu. Plots of the terms in (4.6b) at EC and at CA are given in Fig. 3. As for the nonlinear terms in (4.6b), at both points EC and CA the SD's of NL_1^y and NL_2^y are similar in magnitude and these two terms are fairly well negatively correlated. This similarity in behavior of NL_1^y and NL_2^y appears to indicate that the approximation used in the calculation of NL_2^y may be reasonable. We do find, however, that $NL_2^{y\prime}$ is about twice as large as $NL_1^{y\prime}$ and that NL_1^y is better correlated with $\tilde{Y}_L$ than is NL_2^y. In addition, the correlation of the total nonlinear term NL_A^y with $\tilde{Y}_L$ is near zero and the SD of $\tilde{Y}_T$ is larger than that of $\tilde{Y}_L$. As a result, the accuracy of the estimate of the nonlinear terms is not certain and the amount of balance in $\tilde{Y}_T$ with NL_A^y included is a little questionable. Nevertheless, the calculations should give some indication of the relative magnitude of the nonlinear and the linear terms.

At EC the magnitude of the SD of NL_A^y is substantially less than that of either of the linear terms $f\langle u \rangle$ or $\langle v \rangle_t$. This difference in magnitude is clearly seen in Fig. 3 and should be indicative of the relative importance of these terms at EC. At CA, the relative magnitude of the nonlinear term is somewhat greater, but $NL_A^{y\prime}$ is still smaller than $f\langle u \rangle'$ or $\langle v \rangle_t'$. In general, $f\langle u \rangle$ and $\langle v \rangle_t$ are larger in absolute value than NL_A^y, but during occasional time periods NL_A^y is comparable in magnitude to $\langle v \rangle_t$.

We conclude that the nonlinear terms in (4.6b) are generally smaller than the linear terms $f\langle u \rangle$ and $\langle v \rangle_t$. This appears to hold to a greater extent at the deeper point EC, where the nonlinear terms appear to be small enough to be negligible, than it does at the shallower point CA, where there is an indication that nonlinear effects may not be negligible.

5. Vorticity balance

The extent to which there is a balance of terms in the linear depth-integrated vorticity equation (3.14) is investigated next. The difference approximation to (3.14) is

$$\Delta_x\langle v \rangle_t = (H_x/H_E)R_1(H_y/H_E)R_2, \quad (5.1a)$$

where

$$R_1 = f\bar{u}_B^x + \bar{v}_{Bt}^x - \langle \bar{v} \rangle_t^x, \quad (5.1b)$$

$$R_2 = f\bar{v}_B^x. \quad (5.1c)$$

The effective values of (H_x/H_E) and (H_y/H_E) in (5.1) are not known exactly. To assess the balance, therefore, we calculate the cross correlation coefficients between the three terms $\langle v \rangle_{xt} \approx \Delta_x\langle v \rangle_t$, R_1 and R_2, and we estimate the magnitude of the coefficients (H_x/H_E) and (H_y/H_E) by a linear regression analysis. The values determined from the linear regression are then compared with estimates from the bathymetry to see if the magnitudes are reasonable. Errors from the spatial difference approximations in (5.1) are discussed in Appendix B.

The terms in (5.1) are calculated at the points EC and CA for the same time periods as in Section 4. Measurements at the bottom current meters at each station are used to form $\bar{u}_B^x$ and $\bar{v}_B^x$. The cross correlation coefficients and the standard deviations of the terms $\langle v \rangle_{xt}$, R_1 and R_2 are given in Table 4.

At the point EC, the value of the cross correlation coefficient $\{\langle v \rangle_{xt}, R_1\} = -0.51$ which is reasonably high. The linear regression of $\langle v \rangle_{xt}$ on R_1 at EC gives $(H_x/H_E) = -1.3 \times 10^{-7}$ cm^{-1}. The standard error of this coefficient (see Appendix A) is estimated to be 0.6×10^{-7} cm^{-1}. This value for (H_x/H_E) has the proper order of magnitude and compares fairly well with an estimate from the

TABLE 4. Cross-correlation coefficients and standard deviations from (5.1) at points EC and CA

	EC	CA
$\{\langle v\rangle_{xt}, R_1\}$	−0.51	−0.03
$\{\langle v\rangle_{xt}, R_2\}$	0.22	−0.20
$\{R_1, R_2\}$	−0.56	−0.48
$\langle v\rangle'_{xt}(10^{-11}\ s^{-2})$	4.13	6.12
$R'_1(10^{-4}\ cm\ s^{-2})$	1.61	1.48
$R'_2(10^{-4}\ cm\ s^{-2})$	5.73	9.14

bathymetry of $(\Delta H/\Delta x H_E) \approx -[100\ m/(130\ m \times 15.5\ km)] = -5 \times 10^{-7}\ cm^{-1}$. A plot of $\langle v\rangle_{xt}$ and $(H_x/H_E)R_1$, with $(H_x/H_E) = -1.3 \times 10^{-7}\ cm^{-1}$, is shown in Fig. 4, where the amount of correlation between these two terms may be seen.

At EC, the magnitude of the correlation coefficient $\{\langle v\rangle_{xt}, R_2\}$ is substantially smaller than $\{\langle v\rangle_{xt}, R_1\}$. This indicates that the primary driving term on the right-hand side of (5.1) is $(H_x/H_E)R_1$. Since $R'_2 > R'_1$ mainly because $v'_B > u'_B$, we would expect that if y variations in topography were important in (5.1) a reasonably high correlation of R_2 with $\langle v\rangle_{xt}$ would be obtained. That, however, is not the case. Because of the low value of $\{\langle v\rangle_{xt}, R_2\}^2$, the regression coefficient for (H_y/H_E), which is small in magnitude relative to (H_x/H_E) anyway, is not particularly meaningful and is omitted.

We conclude that the fairly high correlation between $\langle v\rangle_{xt}$ and R_1 and the proper order-of-magnitude estimate of (H_x/H_E) from the regression analysis provide a reasonable amount of evidence to support the existence, in the region between Edelweiss and Carnation, of the linear vorticity balance

$$\langle v\rangle_{xt} = (H_x/H_E)(fu_B + v_{Bt} - \langle v\rangle_t). \quad (5.2)$$

On the other hand, at CA the values of the correlation coefficients $\{\langle v\rangle_{xt}, R_1\}$ and $\{\langle v\rangle_{xt}, R_2\}$ are both small. Evidently, as noted previously in Section 4, there are additional effects, probably frictional, which are operative in the region between Carnation and Aster. These effects are indicated by a general decrease in magnitude of $\langle v\rangle$ at the onshore station Aster, relative to Carnation, as compared with an increase in $\langle v\rangle$ at Carnation, relative to Edelweiss. This variation may be seen from the values of v' at the different stations (Table 1). A comparison of $\Delta_x\langle v\rangle_t$ at EC and CA shows that much of the time this term is of opposite sign at these two points, while R_1 and R_2 generally have the same sign, e.g., $\{\langle v\rangle_{xtEC}, \langle v\rangle_{xtCA}\} = -0.41$, $\{R_{1EC}, R_{1CA}\} = 0.62$. Since the measurements at Aster 44 are only 10 m above the bottom, the decrease in magnitude of $\langle v\rangle$ at Aster may reflect effects from the bottom boundary layer there (Kundu, 1977). Otherwise, frictional effects due to the decrease in depth or to the decrease in horizontal distance from the coastal boundary may act throughout the water column and lower the magnitude of $\langle v\rangle$. In any case, the inviscid vorticity balance (5.1), as approximated here, does not hold at CA.

6. Mass balance

In this section, we investigate to what extent the mass balance constraint (1.6), based on the assumption of two-dimensional motion, holds for the interior flow. Because of the longer time series of measurements at Carnation and Aster, we restrict our attention here to those two stations.

The cross-correlation coefficients between u, at Carnation and Aster, and the wind stress τ are given in Table 5. The maximum value generally occurs within 12 h of zero lag, and the value recorded in Table 5 is the maximum absolute value within the lag time of ±12 h. The time period is the same as in Section 4 for the point AC.

Below 20 m $\{u,\tau\}$ is negative, i.e., a wind stress fluctuation toward the south is generally accompanied by onshore flow, as expected from (1.6). At Carnation, the absolute value of $\{u,\tau\}$ increases with depth and attains its maximum value at the bottom measurement point at 95 m. The values of $\{u,\tau\}$ at 20 m are anomalous, being small and negative at Aster 20 and small and positive at Car 20. This result is an additional indication of surface layer effects at 20 m.

In Kundu and Allen (1976), the u and v velocities from CUE-2 were decomposed, at the individual stations, into vertical empirical orthogonal func-

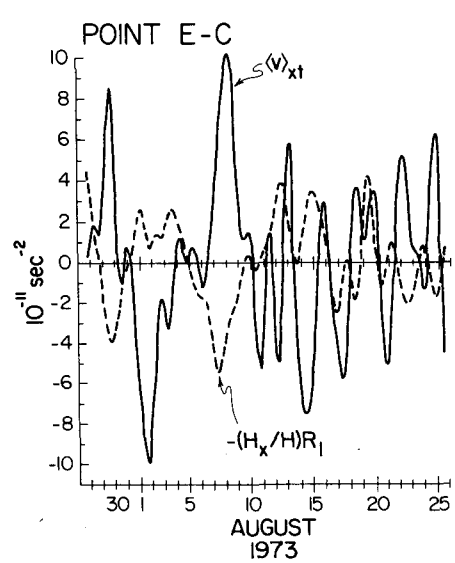

FIG. 4. Time series of $\langle v\rangle_{xt}[= \Delta_x\langle v\rangle_t]$ and $-(H_x/H)R_1$ $[= -(H_x/H_E)R_1]$ in Eq. (5.1) at point EC, where $(H_x/H_E) = -1.3 \times 10^{-7}\ cm^{-1}$.

TABLE 5. Cross-correlation coefficient between u and the wind stress τ (maximum absolute value within lag of ± 12 h).

	Aster		Carnation				
	24	44	20	40	60	80	95
$\{u,\tau\}$	−0.12	−0.38	+0.17	−0.34	−0.34	−0.41	−0.52

TABLE 6. Cross-correlation coefficients (maximum absolute value with lag ± 12 h) and standard deviations (10^4 cm^2 s^{-1}).

$\{U_C,\tau\} = -0.41$	$U'_C = 1.79$
$\{U_A,\tau\} = -0.38$	$U'_A = 0.48$
$\{U_C - U_A,\tau\} = -0.34$	$(U_C - U_A)' = 1.66$
$\{U_C,U_A\} = 0.41$	$(\tau/\rho_0 f)' = 0.49$

tions. It was found that the amplitudes of the first empirical modes for u at Carnation and Aster were very poorly correlated with the wind stress τ. Presumably, this is because the 20 m currents, which also have the largest magnitudes of u' at these stations, were included in the calculation of the empirical modes.

Because of surface layer effects, the depth integral of the interior inviscid onshore velocity is calculated, as before, by integrating over $-H \leq z \leq -H_S$. As a result, Eq. (1.6) becomes

$$U = \int_{-H}^{-H_S} u dz \approx -\tau/f\rho_0, \tag{6.1}$$

where Eq. (4.4) is used to calculate $U = H_E\langle u\rangle$. Subscripts C and A will be used to denote the value of U calculated at Carnation and at Aster, respectively.

The cross correlation coefficients $\{U_C,\tau\}$ and $\{U_A,\tau\}$ are given in Table 6 along with the values of $\{(U_C - U_A),\tau\}$, $\{U_C,U_A\}$ and the standard deviations. If the flow were two-dimensional, $(U_C - U_A)$ would represent the volume flux into the surface layer between Carnation and Aster. The negative values of $\{U_C,\tau\}$ and $\{U_A,\tau\}$ are in agreement with (6.1). The value of $\{U_C - U_A,\tau\}$ is also negative, which indicates that the x gradient of fluctuating onshore-offshore volume flux between Carnation and Aster is consistent with an upwelling motion from the interior into the surface layer when the wind stress has a negative, upwelling-favorable fluctuation.

The correlations between the various U's and τ in Table 6 have the sign expected from (6.1), but their values are not very high. A plot of U_C, U_A, and $\tau/f\rho_0$ versus time is shown in Fig. 5. Since U_A is generally smaller than U_C, the plot of $U_C - U_A$ looks a good deal like that of U_C and is not shown. It is clear from Fig. 5 that the fluctuating values of U_A and $\tau/\rho_0 f$ are similar in magnitude, while the fluctuations of U_C are larger, as indicated by the values of the SD's in Table 6. There are some time periods when the variation of U_C and of U_A appear to be related to that of $\tau/\rho_0 f$ in qualitative agreement with (6.1). For example, this is the case during 11–14 July. Although the magnitudes of U_C and $\tau/\rho_0 f$ do not balance, this supports Halpern's (1976) conclusion about a tendency toward a two-dimensional behavior in the mass balance during that particular time period. At other times, there are time-dependent motions of U_C and U_A which are clearly not correlated with $\tau/\rho_0 f$, e.g., during 19–22 July. These motions are probably associated with

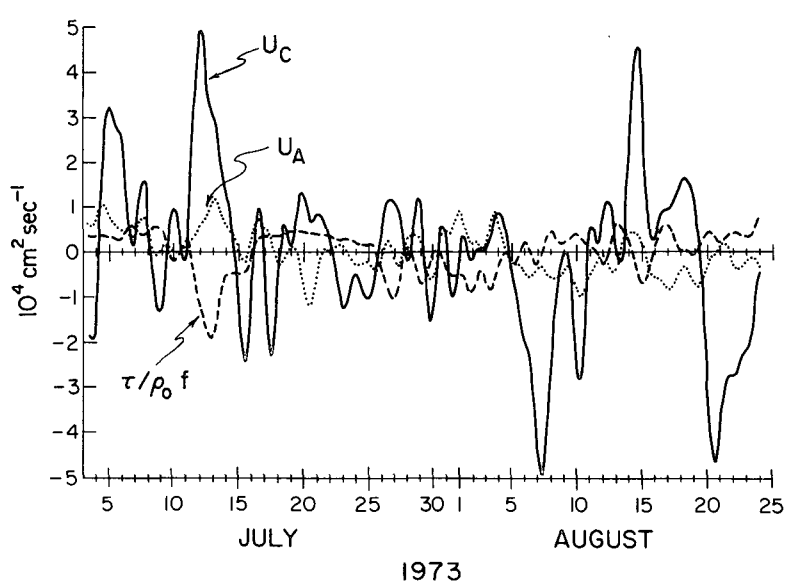

FIG. 5. Time series of U_C,U_A and $\tau/\rho_0 f$.

alongshore gradients in the velocity field, i.e., with three-dimensional effects, inshore of Carnation.

The mean values during this time period are $\overline{\tau/\rho_0 f} = -0.36 \times 10^4$ cm^2 s^{-1}, $\bar{U}_C = 2.10 \times 10^4$ cm^2 s^{-1}, $\bar{U}_A = 0.17 \times 10^4$ cm^2 s^{-1}. The fact that $\bar{U}_C$ is much larger than $-\overline{\tau/\rho_0 f}$ indicates that three-dimensional effects are possibly also important for the mean flow.

Even though the fluctuations U_C and U_A clearly vary in response to processes other than the two-dimensional mass balance in (1.6), it is reasonable to ask what the average, or most likely, values of U_C, U_A and $(U_C - U_A)$ are, over this time period, for different values of $\tau/\rho_0 f$. The answer to that question is best provided by a linear regression of U_C, U_A and $(U_C - U_A)$ on $\tau/\rho_0 f$. The regression coefficients and the estimated standard errors of these coefficients (see Appendix A) are given in Table 7. The values of the coefficients are all close to -1. This result lends support to the general concept of the mass balance (6.1), since it indicates that the part of the U_C which is correlated with τ tends to have a magnitude close to $\tau/f\rho_0$. The relative size of the regression coefficients is also consistent with a vertical flux of mass into the surface layer between Carnation and Aster.

We conclude that there is some evidence that the physics in the two-dimensional mass balance (6.1) is operative, but that there appear to be substantial three-dimensional effects in the u velocity field inshore of Carnation and, possibly, upwelling into the surface layer between Carnation and Aster.

7. Summary

Velocity measurements from the Coastal Upwelling Experiment CUE-2 on the continental shelf off Oregon in the summer of 1973 have been analyzed to investigate whether time-dependent momentum and vorticity balances commonly utilized in theoretical models, and a two-dimensional mass balance, commonly utilized in conceptual models of coastal upwelling, are valid for low-frequency current fluctuations. Measurements from three stations in water of depth 54, 100 and 200 m were utilized.

By a comparison of the magnitude of terms involving horizontal velocities in the linear momentum and nonlinear depth-integrated momentum equations, support is found, in the flow beneath 20 m, for the linear geostrophic balance of the alongshore velocity in the onshore-offshore momentum equation (3.4a) and for a linear ageostrophic balance in the alongshore momentum equation (3.5a). The linear ageostrophic balance (3.5a) appears to hold best in the deeper water of depth 100–200 m. In the shallower water of depth 54–100 m, there is an indication that nonlinear effects may not be negligibly small. There is also some evidence of additional physical processes, probably frictional, entering the momentum balance at the shallowest station at 54 m depth.

Evidence is found to support the validity of the linear, depth-integrated vorticity balance (5.2) between the 100 and 200 m stations. This balance does not appear to hold between 54 and 100 m, presumably due to frictional effects.

The fluctuations in the interior, depth-integrated onshore velocities at 100 and 54 m, U_C and U_A and their difference $(U_C - U_A)$ are shown, from cross-correlation coefficients with the wind stress τ, to have the proper sign to be in accord with the two-dimensional mass balance relation (1.6). The correlation is not particularly high, however, probably due to three-dimensional effects inshore of 100 m.

TABLE 7. Coefficients from the linear regression of dependent variables U_C, U_A and $U_C - U_A$ on $\tau/f\rho_0$.

Dependent variable	Regression coefficient	Standard error
U_C	−1.36	0.70
U_A	−0.37	0.19
$U_C - U_A$	−0.99	0.66

Acknowledgments. This research was supported by the Coastal Upwelling Ecosystems Analysis program (CUEA) of the International Decade of Oceanography office (IDOE) of the National Science Foundation under Grants OCE76-00596 and IDO71-04211 and also (for J. S. Allen) partially by the Oceanography Section, National Science Foundation, under Grant DES75-15202.

The authors thank their CUEA colleagues Dr. R. L. Smith and Dr. R. D. Pillsbury for the use of the CUE-2 current meter data. The first author (J. S. Allen) also thanks Dr. H. L. Bryden for several useful discussions.

APPENDIX A

Statistical Significance of Correlation Coefficients

In the main body of the paper we have listed the values obtained for various cross-correlation coefficients regardless of the magnitude or of the statistical significance from standard tests. Here, for comparative purposes, we give the values of the correlation coefficients at the 10% level of significance for the different length time series involved at the three stations and at the points EC and CA.

An estimate of an integral time scale $\mathcal{T}$, which determines the time period to gain an "independent" measurement and which is appropriate for the cal-

culation of correlation coefficients, is obtained from the equation used by Davis (1976) [see also Eq. (6.71) in Bendat and Piersol (1971)]:

$$\mathcal{T} \approx \sum_{n=-n_0}^{n=+n_0} r_1(n\Delta t) r_2(n\Delta t)\Delta t, \qquad \text{(A1)}$$

where $r_1(t)$ and $r_2(t)$ are the lagged autocorrelation coefficients for variables 1 and 2, respectively, and Δt is the time interval (here 6 h) between data points. The integer n_0 is taken to be large enough that a convergent limit for $\mathcal{T}$ may be estimated. From the appropriate combinations of the autocorrelation coefficients of u, v, τ, and of the other variables used in the calculations, we obtain a general, conservative estimate of $\mathcal{T} \approx 2$ days. The number of independent measurements N_I in a series with N data points is then

$$N_I = N\Delta t/\mathcal{T}. \qquad \text{(A2)}$$

With $\mathcal{T} \approx 2$ days, the number of independent measurements N_I for the calculations involving the velocities at Edelweiss and at EC is $N_I \approx 14.5$ and for the calculations involving the velocities at Aster, Carnation, and CA is $N_I \approx 26$. The corresponding magnitudes of the correlation coefficients, at the 10% level of significance are then 0.45 and 0.33, respectively (Pearson and Hartley, 1970). Many of the larger correlation coefficients referred to in Sections 4–6, especially those at point EC, have magnitudes which are slightly greater than but rather close to these values.

The estimate for N_I is also used in the calculation of the standard error of linear regression coefficients. For example, with N data points for two variables x and y, where x is considered to be the independent variable and where $\bar{x} = 0$, $\bar{y} = 0$, the coefficient b in the regression equation $\hat{y} = bx$ is given by

$$b = \sum^{N} xy / \sum^{N} x^2, \qquad \text{(A3)}$$

and the standard error s_b of b is obtained from

$$s_b^2 = \sum^{N} (y - \hat{y})^2 / [(N_I - 2) \sum^{N} x^2]. \qquad \text{(A4)}$$

APPENDIX B

Errors

Errors involved in the approximation of terms in the equations of motion, with velocity measurements and other observations, have been discussed for particular cases by McWilliams (1976a,b), Bryden (1976) and Bryden and Fofonoff (1977). An attempt is made here to estimate the errors involved in the time difference approximation (4.1) and in the spatial difference and averaging approximation in the linear depth integrated vorticity equation (5.1).

The magnitude of the errors incurred by the use of the time difference approximation (4.1) may be estimated by considering the effect of (4.1) on a sinusoidal signal of frequency ω, e.g., $v = v_0 \exp(i\omega t)$. In that case the square of the ratio of the difference approximation to the true value of the derivative is

$$A_1 = [\Delta_t v / v_t]^2 = [\sin(\omega\Delta t)/\omega\Delta t]^2, \qquad \text{(B1)}$$

where $A_1 \leq 1$ and $A_1 \approx 1$ for $\omega\Delta t \ll 1$. A measure of the relative magnitude of the error variance from the use of (4.1) may be expressed as $A = 1 - A_1$. A calculation of A for some of the higher frequencies present in the low-pass filtered data utilized here gives $A = 0.07, 0.12, 0.19, 0.26$ for $f = (\omega/2\pi) = 0.3, 0.4, 0.5, 0.6$ cpd, respectively. Since A is small over the frequency range of interest and is very small for frequencies $f \leq 0.3$ cpd, where the signals are more energetic, the difference approximation $\Delta_t v$ should provide a reasonably accurate representation of v_t.

We next attempt to estimate the effect of errors in the spatial difference approximation (5.1) to the linear depth-integrated vorticity equation (3.14). The approximation (5.1) contains both the difference and the averaging operators, Δ_x and $\overline{(\ )}^x$.

Let us assume that we have time series measurements of some quantity $\phi(x,t)$ at two points x_1 and x_2 ($x_2 > x_1$), separated by a distance $2\Delta x = x_2 - x_1$ and with the center point $x_0 = \frac{1}{2}(x_1 + x_2)$. Subscripts are used to denote values at measurement points, e.g., $\phi_1 = \phi(x_1)$.

The true values of interest of $\phi(x,t)$ are assumed to vary on spatial scales greater than the separation $2\Delta x$ between the points. Let the measured values be denoted by a subscript m, so that $\phi_m = \phi + \epsilon$, where the error ϵ represents the difference between the measured and the true value of ϕ and is assumed to be due primarily to processes on space scales shorter than $2\Delta x$, but may also be due to unbiased measurement errors. The variables under consideration, therefore, are

$$\phi_{mi} = \phi_i + \epsilon_i, \quad i = 1, 2. \qquad \text{(B2a,b)}$$

It is assumed that all variables have the time mean removed, i.e., $\bar{\phi}_m = \bar{\phi} = \bar{\epsilon} = 0$, and that the errors are random, such that ϕ is uncorrelated with ϵ and that ϵ_1 and ϵ_2 are uncorrelated, i.e.,

$$\{\phi_i, \epsilon_j\} = 0, \quad i, j = 1, 2; \quad \{\epsilon_1, \epsilon_2\} = 0. \qquad \text{(B3)}$$

It follows from (B3) that

$$\overline{\phi_{m1}\phi_{m2}} = \overline{\phi_1\phi_2}, \qquad \text{(B4)}$$

and that

$$\overline{\phi_{m1}^2} = \overline{\phi_1^2} + \overline{\epsilon_1^2}, \quad \overline{\phi_{m2}^2} = \overline{\phi_2^2} + \overline{\epsilon_2^2}. \qquad \text{(B5a,b)}$$

Using the notation

$$r_m = \{\phi_{m1},\phi_{m2}\}, \quad r = \{\phi_1,\phi_2\}, \quad R = r_m/r, \quad \text{(B6a,b,c)}$$

we obtain

$$R^2 = \overline{\phi_1^2}\,\overline{\phi_2^2}/\overline{\phi_{m1}^2}\,\overline{\phi_{m2}^2} \quad \text{(B7a)}$$

$$= [(\overline{\phi_{m1}^2} - \overline{\epsilon_1^2})(\overline{\phi_{m2}^2} - \overline{\epsilon_2^2})]/\overline{\phi_{m1}^2}\,\overline{\phi_{m2}^2}. \quad \text{(B7b)}$$

The first objective is to obtain an estimate of $\overline{\epsilon_i^2}$ from the measurements. These values are then used to estimate the errors involved in the difference and averaging approximations (4.5) which, in terms of ϕ_{mi}, are

$$\phi_x(x_0) = \phi_{x0} \approx \Delta_x\phi_m = (\phi_{m2} - \phi_{m1})/2\Delta x, \quad \text{(B8a)}$$

$$\phi(x_0) = \phi_0 \approx \overline{\phi_m^x} = \tfrac{1}{2}(\phi_{m1} + \phi_{m2}). \quad \text{(B8b)}$$

If an assumption is made which relates $\overline{\epsilon_1^2}$ to $\overline{\epsilon_2^2}$, it is possible to solve (B7) for $\overline{\epsilon_1^2}$ and $\overline{\epsilon_2^2}$ as a function of R. We assume that $\overline{\epsilon^2}$ is a constant, i.e., that

$$\overline{\epsilon_1^2} = \overline{\epsilon_2^2} = \overline{\epsilon_0^2}, \quad \text{(B9)}$$

in which case we obtain

$$\overline{2\epsilon_0^2} = (\overline{\phi_{m1}^2} + \overline{\phi_{m2}^2}) - [(\overline{\phi_{m1}^2} + \overline{\phi_{m2}^2})^2 - \overline{4\phi_{m1}^2\phi_{m2}^2}(1 - R^2)]^{1/2} \quad \text{(B10)}$$

Note that $\overline{\epsilon_0^2} \to 0$ if $R \to 1$, i.e., if $r_m \to r$. For $R \to 0$, $\overline{\epsilon_0^2} \to \min(\overline{\phi_{mi}^2})$.

If it is assumed that ϕ_1 and ϕ_2 are perfectly correlated, i.e., that $r = 1$, then $R = r_m$ and $\overline{\epsilon_0^2}$ may be estimated from measured values by (B10). The processes of interest, i.e., $\phi(x,t)$, may not be perfectly correlated, however. This would be the case, for example, if ϕ was the sum of two or more processes which individually have $r^2 = 1$, but which are mutually uncorrelated. Since the actual values of r are not known, we proceed and obtain approximate values for $\overline{\epsilon_0^2}$ by assuming that $r = 1$. Because $|r| \leq 1$, an overestimate of $\overline{\epsilon_0^2}$ is obtained.

A measure of the relative magnitude of the error variance from the use of (B8a) and (B8b) may be expressed, respectively, as

$$\mathrm{B} = 1 - [(\overline{\Delta_x\phi_m})^2/\overline{\phi_{x0}^2}], \quad \text{(B11a)}$$

$$\mathrm{C} = 1 - (\overline{\phi_m^x})^2/\overline{\phi_0^2}. \quad \text{(B11b)}$$

These may be rewritten in the form

$$B = 1 - B_1B_2, \quad \text{(B12a)}$$

$$C = 1 - C_1C_2, \quad \text{(B12b)}$$

where

$$B_1 = (\overline{\Delta_x\phi})^2/\overline{\phi_{x0}^2}, \quad B_2 = (\overline{\Delta_x\phi_m})^2/(\overline{\Delta_x\phi})^2, \quad \text{(B13a,b)}$$

$$C_1 = (\overline{\phi^x})^2/\overline{\phi_0^2}, \quad C_2 = (\overline{\phi_m^x})^2/(\overline{\phi^x})^2, \quad \text{(B14a,b)}$$

In (B12) the ratios B_1 and C_1 involve errors only from the spatial differencing and averaging approximations of ϕ and depend on the spatial scale of variation of ϕ and on Δx; as $\Delta x \to 0$, $B_1,C_1 \to 1$. On the other hand, the ratios B_2 and C_2 involve the errors ϵ in the measured values ϕ_m. For $\overline{\epsilon^2} \to 0$, $B_2,C_2 \to 1$.

It is convenient to write B_2 and C_2 as

$$B_2 = 1 + b_2, \quad C_2 = 1 + c_2, \quad \text{(B15a,b)}$$

where

$$b_2 = \epsilon_s^2[(\overline{\phi_{m1} - \phi_{m2}})^2 - \overline{\epsilon_s^2}]^{-1}, \quad \text{(B16a)}$$

$$c_2 = \epsilon_s^2[(\overline{\phi_{m1} + \phi_{m2}})^2 - \epsilon_s^2]^{-1}, \quad \text{(B16b)}$$

$$\epsilon_s^2 = \epsilon_1^2 + \epsilon_2^2 = 2\epsilon_0^2. \quad \text{(B16c)}$$

To calculate B_1 and C_1, a representative spatial scale for ϕ must be estimated. We do this in a rough way by assuming that

$$\phi = \phi_0 \exp(\pm kx). \quad \text{(B17)}$$

An exponential rather than a sinusoidal function seems reasonable here since no zero crossings are found in r_m in the onshore-offshore direction. It follows from (B17), that

$$\overline{\phi_1^2}/\overline{\phi_2^2} = \exp(\pm 4k\Delta x), \quad \text{(B18)}$$

$$B_1 = (\sinh k\Delta x/k\Delta x)^2, \quad \text{(B19a)}$$

$$C_1 = (\cosh k\Delta x)^2. \quad \text{(B19b)}$$

With (B5) and (B10), $k\Delta x$ may be found from (B18).

For (5.1), we are interested in estimating B and C in (B12) with

$$\phi = \langle v\rangle_t \text{ in (B12a)}, \quad \phi = R_1 \text{ in (B12b)}. \quad \text{(B20)}$$

The relevant variances, cross-correlation coefficients and calculated values of $\overline{\epsilon_0^2}$, $k\Delta x$, B_1, C_1, b_2 and c_2 for $\Delta_x\langle v\rangle_t$ and R_1, as appropriate, are given in Table 8.

The estimates for B_1 and C_1 are close to 1 and indicate that the errors from the finite-difference

TABLE 8. Variances, cross-correlation coefficients and calculated values from Eqs. (B10), (B16), (B18), and (B19). The subscripts E and C denote measured values of Edelweiss and Carnation, respectively, and replace the subscripts $m1$ and $m2$.

$\overline{\langle v\rangle_{tE}^2} = 39.3 \times 10^{-10}$ cm^2 s^{-4}	$\overline{\langle v\rangle_{tC}^2} = 87.3 \times 10^{-10}$ cm^2 s^{-4}
$\overline{R_{1E}^2} = 5.29 \times 10^{-8}$ cm^2 s^{-4}	$\overline{R_{1C}^2} = 2.33 \times 10^{-8}$ cm^2 s^{-4}
$\{\langle v\rangle_{tE},\langle v\rangle_{tC}\} = 0.73$	$\{R_{1E},R_{1C}\} = 0.39$
For $\langle v\rangle_t$	For R_1
$\overline{\epsilon_0^2} = 14.3 \times 10^{-10}$ cm^2 s^{-4}	$\overline{\epsilon_0^2} = 1.79 \times 10^{-8}$ cm^2 s^{-4}
$k\Delta x = 0.27$	$k\Delta x = 0.47$
$B_1 = 1.02$	$C_1 = 1.24$
$b_2 = 2.27$	$c_2 = 0.52$
$B = -2.34$	$C = -0.88$

and averaging approximation alone are small, with the larger error indicated for the averaged term R_1.

The estimated value of b_2 is greater than 1, which implies for $\Delta_x\langle v\rangle_t$ that the error variance is larger than the signal variance. As noted before, however, the values of $\overline{\epsilon^2}$ obtained by assuming $r = 1$ are likely overestimates which leads, of course, to an overestimate for b_2. Nevertheless, this result provides an indication of the possible extent of the errors involved when straightforward difference approximations are utilized.

With estimates of B_2 and C_2 for $\langle v\rangle_t$ and R_1 it is possible to proceed and to estimate the effect of the errors in the calculation of $\Delta_x\langle v\rangle_{tm}$ and $\tilde{R}^x_{1m}$ on the correlation coefficient

$$\tilde{r}_m = \{\Delta_x\langle v\rangle_{tm}, \tilde{R}^x_{1m}\}. \tag{B21}$$

Utilizing an analysis similar to that which led to (B7), we obtain

$$\tilde{r}_m = \tilde{r}(B_2C_2)^{-1/2}, \tag{B22}$$

where $\tilde{r} = \{\Delta_x\langle v\rangle_t, \tilde{R}^x_1\}$ and where B_2, C_2 are obtained using (B20). If we assume perfect correlation between the difference approximations to these two terms, i.e., $\tilde{r}^2 = 1$, and use values of B_2 and C_2 calculated with (B15) from Table 8, we find $|\tilde{r}_m| = 0.45$. This estimate is less than, but comparable to, the value $|r_m| = 0.51$ found in Section 5. The fact that $|\tilde{r}_m| < |r_m|$ is probably due to an overestimate of the errors in b_2 and c_2.

Since $|\tilde{r}_m| > 0.45$ if $r^2 < 1$ for $\langle v\rangle_t$ or R_1, but $|\tilde{r}_m| < 0.45$ if $\tilde{r}^2 < 1$, an estimate of a lower bound for $|\tilde{r}_m|$ has not been found. The analysis indicates, however, that if the errors in $\Delta_x\langle v\rangle_t$ and R_1 are as large as the estimates there is still a possibility of finding a value of $|\tilde{r}_m|$ approximately as large as 0.45 if $\tilde{r}^2 \approx 1$. If the errors are close to those obtained from the estimates, it follows that $\langle v\rangle_{xt}$ and R_1 must have a reasonably high correlation in order for the measurements to give a value of $|\tilde{r}_m| = 0.51$.

REFERENCES

Allen, J. S., 1975: Coastal trapped waves in a stratified ocean. *J. Phys. Oceanogr.*, **5**, 300–325.

——, 1976: Some aspects of the forced wave response of stratified coastal regions. *J. Phys. Oceanogr.*, **6**, 113–119.

Bendat, J. S. and A. G. Piersol, 1971: *Random Data: Analysis and Measurement Procedures*. Wiley-Interscience, 407 pp.

Bryden, H. L., 1976: Horizontal advection of temperature for low-frequency motions. *Deep-Sea Res.*, **23**, 1165–1174.

——, and N. P. Fofonoff, 1977: Horizontal divergence and vorticity estimates from velocity and temperature measurements in the MODE region. *J. Phys. Oceanogr.*, **7**, 329–337.

Davis, R. E., 1976: Predictability of sea surface temperature and sea level pressure anomalies over the North Pacific Ocean. *J. Phys. Oceanogr.*, **6**, 249–266.

Gill, A. E., and A. J. Clarke, 1974: Wind induced upwelling, coastal currents and sea level changes. *Deep-Sea Res.*, **21**, 325–345.

——, and E. H. Schumann, 1974: The generation of long shelf waves by wind. *J. Phys. Oceanogr.*, **4**, 83–90.

Halpern, D., 1976: Structure of a coastal upwelling event observed off Oregon during July 1973. *Deep-Sea Res.*, **23**, 495–508.

Huyer, A., 1976: A comparison of upwelling events in two locations: Oregon and Northwest Africa. *J. Mar. Res.*, **34**, 531–546.

——, B. M. Hickey, J. D. Smith, R. L. Smith and R. D. Pillsbury, 1975: Alongshore coherence at low frequencies in currents observed over the continental shelf off Oregon and Washington. *J. Geophys. Res.*, **80**, 3495–3505.

Kundu, P. K., 1976: Ekman veering observed near the ocean bottom. *J. Phys. Oceanogr.*, **6**, 238–242.

——, 1977: On the importance of friction in two typical continental waters: off Oregon and Spanish Sahara. *Bottom Turbulence*, J. C. J. Nihoul, Ed., 8th Liege Colloquium on Ocean Hydrodynamics (1976), Elsevier, 187–207.

——, and J. S. Allen, 1976: Some three-dimensional characteristics of low frequency current fluctuations near the Oregon coast. *J. Phys. Oceanogr.*, **6**, 181–199.

——, J. S. Allen and R. L. Smith, 1975: Modal decomposition of the velocity field near the Oregon coast. *J. Phys. Oceanogr.*, **5**, 683–704.

McWilliams, J. C., 1976a: Maps from mid-ocean dynamics experiment: part I. Geostrophic streamfunction. *J. Phys. Oceanogr.*, **6**, 810–827.

——, 1976b: Maps from mid-ocean dynamics experiment: part II. Potential vorticity and its conservation. *J. Phys. Oceanogr.*, **6**, 828–846.

Pearson, E. S., and H. O. Hartley (Editors), 1970: *Biometric Tables for Statisticians*, Vol. 1. Cambridge University Press, 270 pp.

Pillsbury, R. D., J. S. Bottero, R. E. Still and W. E. Gilbert, 1974: A compilation of observations from moored current meters, Vols. VI and VII. Refs. 74-2 and 74-7, School of Oceanography, Oregon State University.

Smith, R. L., 1974: A description of current, wind and sea-level variations during coastal upwelling off the Oregon coast, July-August 1972. *J. Geophys. Res.*, **79**, 435–443.

Walin, G., 1972: On the hydrographic response to transient meteorological disturbances. *Tellus*, **24**, 169–186.

Wang, D. P. and C. N. K. Mooers, 1976: Coastal trapped waves in a continuously stratified ocean. *J. Phys. Oceanogr.*, **6**, 853–863.